CrossMark

Development of the Primary Sorption Pump for the SEIS Seismometer of the InSight Mission to Mars

Mihail P. Petkov[1] · Steven M. Jones[1] · Gerald E. Voecks[1] · Kenneth J. Hurst[1] ·
Olivier Grosjean[2] · Delphine Faye[2] · Guillaume Rioland[2] · Cecily M. Sunday[1] ·
Emma M. Bradford[1] · William N. Warner[1] · Jerami M. Mennella[1] · Ned W. Ferraro[1] ·
Manuel Gallegos[1] · David M. Soules[1] · Philippe Lognonné[3] · W. Bruce Banerdt[1] ·
Jeffrey W. Umland[1]

Abstract We report on the development of a passive sorption pump, capable of maintaining high-vacuum conditions in the InSight seismometer throughout the duration of any extended mission. The adsorber material is a novel zeolite-loaded aerogel (ZLA) composite, which consists of fine zeolite particles homogeneously dispersed throughout a porous silica network. The outgassing species within the SEIS evacuated container were analyzed and the outgassing rate was estimated by different methods. The results were used to optimize the ZLA composition to adsorb the outgassing constituents, dominated by water, while minimizing the SEIS bakeout constraints. The InSight ZLA composite additionally facilitated substantial CO_2 adsorption capabilities for risk mitigation against external leaks in Mars atmosphere. To comply with the stringent particle requirements, the ZLA getters were packaged in sealed containers, open to the SEIS interior through 1 µm-size pore filters. Results from experimental validation and verification tests of the packaged getters are presented. The pressure forecast based on these data, corroborated by rudimentary in situ pressure measurements, infer SEIS operational pressures not exceeding 10^{-5} mbar throughout the mission.

The InSight Mission to Mars II
Edited by William B. Banerdt and Christopher T. Russell

✉ M.P. Petkov
mihail.p.petkov@jpl.nasa.gov

[1] NASA Jet Propulsion Laboratory, California Institute of Technology, 4800 Oak Grove Drive, Pasadena, CA 91109, USA

[2] Centre National d'Études Spatiales (CNES), 18 avenue Edouard Belin, 31401 Toulouse, France

[3] Equipe de Géophysique Spatiale et Planétaire, Institut de Physique du Globe de Paris, 94100 Saint Maur des Fossés, France

Abbreviations

CAD   Computer-aided design
EC   Evacuated container
EDX   Energy dispersive X-ray
EOL   End-of-life
FAU   Faujasite zeolite
JPL   Jet Propulsion Laboratory
PAL   Pressure at launch
PCL   Particle cleanliness level
PQV   Packaging qualification and verification
PTFE Polytetrafluoroethylene
RGA   Residual gas analyzer
RT   Room temperature
SEIS Seismic Experiment for Interior Structure
SEM   Scanning electron microscopy
SP   Short-period seismometer
SRS   Shock response spectrum
TGA   Thermo-gravimetric analysis
UHV   Ultra-high vacuum
VBB   Very broad band sensor
ZLA   Zeolite-loaded aerogel
XRF   X-ray fluorescence
V&V   Validation and verification

1 Introduction

The InSight mission to Mars is focused on understanding the interior of another planet using a suite of complementary techniques. The primary experiment is carried out with a sensitive seismometer, Seismic Experiment for Interior Structure (SEIS), whose goal is to detect seismic signals from quakes, meteor impacts, landslides, and atmospheric disturbances. Detection and analysis of these signals will be used to infer the interior structure of Mars (De Raucourt et al. 2012; Mimoun et al. 2012; Dehant et al. 2012; Lognonné and Johnson 2015; Panning et al. 2016; Banerdt et al. 2017).

SEIS consists of an oblique 3-axis very broad band (VBB) seismometer and a 3-axis short period (SP) seismometer. The VBB sensor noise level is below 10^{-9} m/s^2/Hz$^{1/2}$ over the band from 0.1–1 Hz horizontally and 0.01–1 Hz vertically. The SP sensor noise is below 10^{-8} m/s^2/Hz$^{1/2}$ from 0.1–1 Hz (Mimoun et al. 2017). These noise levels are similar to high-quality terrestrial seismometers. To maintain these characteristics on Mars, the VBB sensors are enclosed in an evacuated container (EC) and must operate under high vacuum conditions, conventionally defined as 10^{-2} to 10^{-6} mbar.

The largest sources of noise for SEIS will be due to the operational environment. On Earth, environmental noise is usually mitigated by burial of the seismometer below ground and maintaining a constant temperature environment. On Mars, SEIS will be deployed from the deck of the lander and placed on the ground without having the capability to bury it, leaving it exposed to thermal difference and wind pressure. The ambient diurnal temperature range at the planet surface can approach 100 °C, which precludes nominal operations. It is essential for the detection performance that any change in the temperature of the pendulums be kept to a minimum. The implemented thermal protection scheme, in conjunction with

the high vacuum in the EC, helped achieve time constant at the VBB sensors with respect to the ambient temperature greater than 11 hours. Indeed, the presence of gas in the EC at pressures $> 10^{-4}$ mbar would create direct thermal path from the VBBs to the EC shell, thereby lowering the instrument thermal constant.

The nominal operation of the VBB sensors also requires a large quality factor (Q factor), which facilitates their high gain and broad bandwidth. That is ensured by $< 10^{-4}$ mbar pressure in the EC, which virtually eliminates the Brownian noise and viscous damping of the VBB sensors. A reduction of the Q factor suppresses the sensitivity to faint seismic signals and SEIS ceases to operate satisfactorily at $Q \sim 10$ corresponding to pressures exceeding ~ 0.3 mbar.

The SEIS end-of-life (EOL) pressure requirement has been defined as 0.1 mbar, based on the thermal noise, Brownian noise, and viscous damping requirements. The best science return from the seismometer needs pressures below 10^{-4} mbar, at which the environmental noise components and VBB damping become negligible. Such vacuum, however, is unattainable without the implementation of on-board pumping. The instrument outgassing rate was rather high despite the use of low total-mass-loss adhesives in the VBB construction and the additional steps taken to further reduce their outgassing. Without pumping, the gas load would cause a pressure increase exceeding the EOL pressure requirement within 40 days at ambient temperature. This outgassing behavior was obscured by a large leak in the electrical feedthrough in the initial design of the seismometer that developed during thermal cycling. This internal outgassing combined with an external leak forced delay of the launch from 2016 to 2018. During this two-year delay, the EC was redesigned and the getters described in this paper were developed and implemented.

The implementation of any kind of mechanical pump involving moving parts was not feasible because any such mechanism would cause noise several orders of magnitude above the anticipated quake signals. Ion pumps create strong magnetic fields that may interfere with the sensors performance, whereas non-evaporative getters (NEG) require at least 450–600 °C activation temperatures that were difficult to implement while keeping the VBBs temperature exposure within allowable limits. NEG also have limited adsorption capacity for organic volatiles. Furthermore, both ion pumps and NEG have inadequate capacities to cope with large outgassing rates. In addition, tight mass constraints limited any solution to about 100 grams.

In this paper we report on the formulation, development and implementation of unique zeolite-loaded aerogel (ZLA) getters in lieu of a primary sorption pump for the SEIS instrument. We describe: the process of adsorbent material selection, choice of implementation form, packaging aspects, adsorption testing, and development and optimization of the getters performance characteristics tailored to the seismometer needs. The goal of this sorption pump development was to facilitate the best science return by maintaining $< 10^{-4}$ mbar pressure throughout the duration of the mission. The resulting sorption pump for SEIS complied with all non-vacuum-related environmental requirements.

2 Vacuum Requirements

2.1 End-of-Life Pressure and Vacuum Budget

Some aspects of the SEIS vacuum requirements that deviate from the conventional considerations warrant a discussion. Usually, the pressure inside a sealed vacuum vessel increases with time due to leaks (external or virtual), and/or deterioration of the pumping efficiency. It

Table 1 Allocation distribution of the 0.1 mbar PAL budget

Pressure budget (mbar)	Allocation
0.01	**Outgassing and getter adsorption balance**
0.01	External leaks in 1 atmosphere air/N_2
0.03	Trapped 1 atmosphere air in dead volume
0.05	Margin

is thus reasonable to expect that the worst vacuum conditions would be reached at the end of the mission. Following all nominal processes along the SEIS timeline, however, the worst-case pressure in the sealed instrument is encountered at around the time of launch. In the absence of a real or virtual leak, the internal pressure is governed by outgassing mainly from adhesives. The diffusion of species through bulk epoxy resins carries a strong temperature dependence. Thus, room temperature (RT) outgassing throughout the period between sealing and launch vastly dominates the pressure contribution. At mission operating conditions on Mars, the outgassing will be drastically reduced. Furthermore, the gas pressure in SEIS will decrease in accordance with thermodynamic laws and due to enhanced getter adsorption on cold intrinsic surfaces. The pressure throughout the primary mission is forecasted to be at least two orders of magnitude lower than that at launch.

Similarly to the outgassing considerations, a pressure increase prior to launch due to a defect causing a real leak carries a larger threat than the same defect on Mars. Since leak rates in the medium to high vacuum range scale with the external pressure, which on the Mars surface is only 1% of that on Earth, a significantly higher leak tolerance throughout the mission exists should the seal be compromised after landing. No pressure increase occurs through a compromised seal in the vacuum of space.

Considerations of all vacuum-related phenomena lead us to infer that the worst-case SEIS pressure is reached at around the time of launch. Although it is conceivable to accept pressures > 0.1 mbar at launch and still guarantee acceptable vacuum in the EC on Mars due to the lower operational temperature, such arguments necessitate extensive and complex justification. Here we adopted a significantly more stringent but simple limitation by applying the EOL pressure requirements to the pressure at launch (PAL). In effect, this guarantees high-vacuum environment in the seismometer for the duration of any extended mission. EOL pressure will not be met for many decades on Mars.

The PAL budget of 0.1 mbar was distributed among specific allocations (Table 1), which account for pressure contributions from all possible sources over a period of 14 months (the time from sealing the instrument 8 April 2017 to the end of the launch window 8 June 2018). Each of the gas-contribution allocations carries a significant additional margin not specified in Table 1. This article deals with the pressure balance between material outgassing and getter adsorption (bold).

The unvented (dead) volume accounts for several blind holes on VBB sensor components with no designed path for gas flow into the SEIS vessel. Redesign was not a viable option at the late stage of the seismometer development when the design implications were realized. Although experimentation with representative cases showed that trapped air was evacuated through leak paths along fastener threads, such outcome cannot be guaranteed. This remains the largest albeit unlikely threat to the vacuum budget as its allocation exceeds the optimum sensor performance pressure, and nitrogen is not efficiently adsorbed by the ZLA getters at the operating temperatures. This vacuum budget portion accounts for the possibility that trapped air at atmospheric pressure in the dead volume can escape at any time and expand

into the 3.3 L container. The 0.03 mbar allocation resulted from the cumulative volume estimated from a CAD model; a direct measurement was not possible.

The distribution of the external leak budget over 14 months at RT results in a maximum tolerable mass flow rate of 9×10^{-10} mbar L/s standard air, which is equivalent to 2.4×10^{-9} mbar L/s atm.-He leak rate. The entire SEIS instrument has been leak-tested to $< 10^{-10}$ mbar L/s atm.-He throughout the full temperature range except for the final pinchoff seal, which is impossible to test. The pinchoff process has also been verified to the same criterion. Thus, any external leak contribution to the pressure budget is highly improbable.

The only credible pressure contribution comes from the component outgassing relative to the getter adsorption rate and capacity. The gas load and its removal through pumping is the foundation for any conventional vacuum system design and it usually accounts for the entire vacuum budget. Virtual leaks are excluded through design, real leaks—through testing, and margin is built in with adequate pumping. In an analogy applied to SEIS, had blind holes been eliminated through design, the maximum contribution due to undetectable-through-test external leaks would have been insignificant (0.0004 mbar standard air), and the respective 0.01 mbar allocation would have been the entire budget, guaranteed with sufficient margin.

2.2 Outgassing Species and Rate

The SEIS outgassing constituents were identified using a residual gas analyzer (RGA) during multiple evacuation and bakeout events. The RGA spectra at high temperature (115 °C) were dominated by organic species attributed to residual byproducts of adhesives curing processes. Considering the ionization efficiencies for water (1.12) and organics (typically, 3–4), the factor with which species are overrepresented in an RGA spectrum with respect to N_2, the volatile organics gas load at 115 °C was estimated to be roughly equal to that of the water. Upon cooling, the organics contribution decreased abruptly below 106 °C, and then diminished exponentially with the further reduction of temperature. This behavior is consistent with a phase transition of polymers marked by a glass transition temperature, T_g. The free volume in polymers increases sharply above T_g, which creates diffusion channels for crosslinking fragments that were otherwise trapped in the solid network to escape from the adhesive bulk. This phenomenon was used to identify the culprit—Henkel Ablefilm 550 adhesive film, whose glass transition temperature was listed at 105 °C. A total of 0.18 g Ablefilm 550 was used in a critical location of the VBB pivot where implementing alternatives was impractical. Thus, to significantly reduce the volatile organics gas load, as well as from sensor-related mechanical stress considerations, the maximum bakeout temperature for the reworked SEIS instrument was limited to 100 °C, below the T_g of Ablefilm 550.

Volatile organics are adsorbed efficiently by zeolite materials and could thereby compete with water for getter capacity. This threat, which existed during bakeout, was drastically reduced through an engineered conductance scheme rather than getter capacity allocation. The molecular conductance of the pinchoff tube (queusot), through which the instrument was evacuated, was approximately 2 L/s. Each of the getters, which were encapsulated in canisters (details are given in Sect. 4) opened to the SEIS interior through filters, whose molecular flow conductance was of the order of 0.01 L/s. Thus, most of the gas load during the SEIS bakeout step was directed outward to the external pumping system.

At RT, the species represented in the RGA spectrum were H_2, H_2O, CO, and CO_2. No other significant peaks were detected. All of these species can be largely attributed to the presence of water vapor. The ~ 2100 °C hot tungsten filaments of the RGA induce water cracking and facilitate chemical reactions of the fragments with impurities in the tungsten,

mainly carbon. These are well-understood phenomena, known to produce H_2 and copious amounts of CO and CO_2 (O'Hanlon 2003). Although quantification of the RGA spectrum is not straightforward, we argue that the combined contribution of non-water gas sources was several percent.

The total outgassing rate at RT was evaluated indirectly under quasistatic conditions during bakeout events of the original and rebuilt instrument (in 2015 and 2017), as well as in a direct measurement of a spare instrument containing one VBB sensor in 2016 (Grosjean et al. 2018). The former method relied on external pressure measurement, RGA data, and calculations of the conductance characteristics of the pumping manifold. The latter approach was a more direct pressure-rise measurement method also using external pressure sensors; however, it did not include the full set of outgassing components. Both results yielded an outgassing rate consistent with 1×10^{-7} mbar L/s within a factor of two uncertainty. This is a reasonable agreement, considering the instrument design, the restricted gas conductance through the queusot, the outgassing contribution of external vacuum hardware, and the lack of intrinsic pressure sensor, all of which impacted the accuracy of the estimates. This outgassing rate was significant even for an instrument with medium vacuum requirements (0.1 mbar EOL). In the absence of a pumping mechanism, the pressure due to such gas load in the 3.3 L SEIS volume exceeds the outgassing pressure allocation budget within ~ 4 days at RT after sealing, and the PAL limit within ~ 40 days.

2.3 Getter Approach

A direct measurement of the H_2 outgassing from the metal components in the SEIS instrument was hindered by several factors. Specific H_2 outgassing rates for stainless steel reported in the literature vary by several orders of magnitude depending on the treatment conditions. Ti alloys, the H_2 outgassing from which is governed by intergranular diffusion, exhibit similar variability depending on the material microstructure. As the outgassing mechanisms in the two metals are very different, agreement is lacking even for the same heat treatment condition, showing stronger outgassing from stainless steel ranging between 30 and 240 (Takeda et al. 2011). Additionally, all EC Ti-6Al-4V components were vacuum-annealed at 320 °C for 24 hours, which is known to reduce the outgassing from the Ti alloy by more than an order of magnitude. The combined effect of the above factors was the dominant H_2 outgassing background from the external to the EC vacuum pumping manifold, despite that Ti-6Al-4V made the largest contribution to the surface area. Furthermore, quantification of outgassing from the RGA filaments and the water reactions on them was not straightforward. Effectively, our measurements placed a very conservative estimate of the H_2 outgassing rate at $\sim 10^{-9}$ mbar L/s. Unaddressed, this would lead to pressure accumulation of ~ 0.01 mbar H_2 at the time of launch (< 0.01 mbar throughout the mission). Even though such pressure buildup can be accommodated by the SEIS vacuum budget, a H_2 getter was implemented for risk reduction.

In lieu of a H_2 getter we chose Rel-Hy® available from SAES Getters—a double Pd/Ti thin film made using a proprietary process, accommodating deposition on custom substrates. This H_2 getter is ineffective for water and organics and was thus uncompromised during bakeout. Two discs with a combined area of > 80 cm^2 were coated on both sides by SAES Getters and were subsequently welded on each of the EC shells. The specific H_2 capacity of 3 cm^3 Torr/cm^2, measured on witness coupons, was sufficient to cope with $> 6 \times 10^{-9}$ mbar L/s H_2 outgassing rates. This significantly exceeded any realistic outgassing estimate at RT.

The Pd coating of the Pd/Ti film had emissivity of ~ 0.05 and the H_2 getter discs doubled as additional redundant thermal shields.

RT water outgassing from adhesives was the principal threat to the vacuum requirements and thus became the primary adsorption target governing the getter functionality. Considering the minor contribution from all other sources, we argue that the water adsorption capability of a getter, in conjunction with the reduced outgassing and pressure reduction at the mission operating temperatures, was a sufficient requirement for complying with the SEIS vacuum requirements. Water adsorption was realized through zeolite-based getters, whose development, implementation and integration are the crux of this article. Adhesive curing processes can produce CO and CO_2 crosslinking byproducts, whose plausible gas load contributions were also considered. CO/CO_2 adsorption capabilities were implemented for risk reduction.

3 Zeolite-Loaded Aerogel Composites

3.1 Zeolite Characteristics

Zeolites emerged early on as an appealing getter material option. These are aluminosilicate materials with controlled porosity, some varieties of which contain vast amounts of water in their hydrated state. Zeolites are obtained by the polymeric combination of quartz-like TO_4 tetrahedra, where T is either Si or Al. The multitude of possibilities of connecting these tetrahedra into large crystalline structures, as well as the silicon to aluminum molar ratio of the microporous framework, results in a broad spectrum of zeolite varieties.

The incorporation of Al into the zeolite framework induces the generation of an intrinsic Brönsted acidity which, coupled with a typical high thermal stability, is responsible for their interesting adsorption and catalytic properties. Charge neutrality upon substitution of Si^{4+} with Al^{3+} is achieved by the entrapment of positive ions, such as H^+, Na^+, K^+, Ca^{2+}, Cu^{2+} or Mg^{2+}. These ions strongly influence the adsorption characteristics for specific adsorbates and enhance the retention time of some molecules at high temperature and/or under vacuum. For example, Mg^{2+} and Ca^{2+} enhance the adsorption of organic volatiles, CO and CO_2. Ion exchange reactions can be utilized to further enhance the abundance of a preferred cation to more efficiently trap a targeted adsorbate.

The materials selected for InSight were synthetic faujasite-type (FAU) zeolite 13X due to their large water capacity in the hydrated state and market abundance of zeolite 13X varieties with different cations (H^+, Na^+, Ca^{2+}, Mg^{2+}, etc.), having different sensitivities to adsorbates. FAU, whose empirical chemical formula is $[Ca_x,Mg_y,(Na_2)_z(H_2O)_{240}][Al_{58}Si_{134}O_{384}]$ with $x + y + z = 29$, contains significant amount of moisture. FAU is constructed of truncated octahedra, referred to as sodalite cages, each built with 24 TO_4 tetrahedra. The sodalite cages are connected with aluminosilicate bridges (known as d6R), resulting in a face-centered cubic (fcc) structure. The pores contained in the sodalite cages, and the supercages in the center of each fcc unit cell, comprise the porosity. Water molecules are adsorbed in front of each cation, and molecular access to the adsorption sites is governed by the microstructure. FAU has one of the most open structures among zeolites, and the linear "channels" in the fcc arrangement enhance molecular diffusion.

Synthetic zeolite 13X (FAU) can be prepared from a wide range of $SiO_2:Al_2O_3$ mole ratios, generally categorized as X (ratio < 3) and Y (ratio > 3) types. Fine-tuning of the desired zeolites properties can be done by ion exchange reactions to substitute the most abundant Na^+ ions with another cation. The synthetic zeolite 13X are identified by the exchanged cation type (H, Na, Ca, Mg, etc.), and X or Y for the $SiO_2:Al_2O_3$ mole ratio category. In

the course of the development of the SEIS getters we used commercially available HY, NaY, and CaX zeolite 13X (Petkov et al. 2018b).

Zeolites materials are widely used in cryogenic sorption pumps. One gram of cryogenically cooled zeolite material would suffice to pump the air from the SEIS instrument volume from atmospheric pressure down to 10^{-2} mbar in several minutes. Their vacuum performance at ambient temperatures is not extensively characterized due to the lack of such applications. However, literature data suggest that the propensity for water adsorption of dehydrated zeolites remains high and they would be adequate to maintain medium to high vacuum under moderate gas loads. Complete dehydration requires very high temperatures, but the majority of the moisture ($\sim 80\%$) is efficiently removed during extended exposure to the typical bakeout temperatures of vacuum instruments, around 100 °C. Relevant to SEIS, no special material conditioning is necessary and the getters adsorption capacity is generated during the final instrument bakeout step at 100 °C prior to sealing it.

The zeolites are virtually unaffected by harsh space environments. Conventional cryogenic applications typically cover the $-195°C$ to $+350$ °C temperature range, which makes them exceptionally suited to the Mars and other icy worlds conditions. The materials are stable in diverse environments and do not impose any lifetime restrictions on the use as getters. With the implementation of suitable decontamination process, they can be reused a large number of times under extreme thermal cycles without compromising their efficiency. The performance in mechanical shock and vibration environments is determined by the implementation method, not the zeolite particles, as the bulk minerals can withstand significant stresses.

3.2 Zeolite Implementation Concepts

The implementation of zeolite materials could take on different forms, but instrument requirements that were unrelated to vacuum quality provided significant challenges. A common use of zeolites in sorption pumps is in the shape of pellets, made of bonded particles with a permeable material, facilitating molecular diffusion to the adsorption sites. Such products were developed by CNES for the ChemCam and instrument on the Mars Curiosity rover (Faye et al. 2010), and later for SuperCam for Mars 2020 (Rioland et al. 2016). The packaging of these zeolite pellets utilized quartz wool that generated a significant particulate contamination. This approach was deemed unattractive for SEIS because of the risk posed by particles to critical functions of the VBB sensors.

Alternative methods relied on deposition of zeolites on the surface of porous open-cell metallic foams, which provided large surface area and excellent accessibility through open porosity network. Fecralloy, an iron alloy with 20–22% Cr and 5% Al, emerged as a primary choice due to its extensive use in catalytic applications. Prototype samples exhibited superb zeolite adhesion, excellent binder permeability, and high zeolite adsorption efficiency. However, the Fecralloy ferromagnetic properties were deemed harmful to the VBBs operation. The attempts to substitute Fecralloy with similarly shaped open-cell Al 6061 foam presented zeolites adhesion challenges. The growth of dendritic α-alumina on Fecralloy surface at 900 °C facilitates excellent zeolite bonding; however, Al alloys melt at such temperatures. A lower temperature heat treatment of Al 6061 produces γ-alumina, which is less conducive to binder adhesion. While the implementation of the Al 6061 foam was feasible, it required significant development efforts that would have adversely impacted the already constrained project schedule.

Ultimately, a composite zeolite-loaded aerogel material was devised and developed for InSight (details are given in Sect. 5). This built on prior experience in fabricating aerogel

matrices with dispersed particle loads of colloidal graphite, nanospheres, magnetic particles, etc. The resulting microstructure was sparsely distributed micron-sized zeolite particles, embedded in the solid silica aerogel network with a fully interconnected open porosity providing adequate molecular access to the zeolites. The homogeneous zeolite dispersion ensured maximum adsorption efficiency. There was no binder that can partially seal the surface of the zeolite particles, and the large aerogel mesopores facilitated significantly faster molecular transport than any microporous polymeric binder material. The ZLA composite was fabricated from a liquid precursor, which can be cast in almost any shape. This aided the getter implementation and utilized available spaces in custom designed containers.

4 Getter Packaging

4.1 Container Design

The objective of the getter packaging design was to provide a structural container for a passive getter solution while maximizing the available volume for the getter material. The final form of the packaging elements was driven by the need to maintain an overall mass comparable to that of the original getter design, to maintain the same mounting interface as the original design, to respect the keep-out volumes of the EC structures and VBB sensor elements, and to prevent loose particulates from entering the Evacuated Container. During the re-work phase of the SEIS instrument build, the design of the getter structures and the development of the new getter material took place in parallel. Consequently, the getter structures were designed for compatibility and ease-of-assembly with a variety of getter types, including metallic foam, compacted pellets and ZLA composites. Robust titanium structures combined with a secure particle filter permitted the getter assemblies to withstand the mission's thermal, shock, and vibration environment, independent of the form or structural integrity of the getter material.

The getter elements in the re-worked EC maintained the same configuration and mounting interfaces as in the original instrument design. As shown in Fig. 1, the EC held a total of six getter assemblies, three clustered at the center of the sphere, and three exterior ones equally spaced around its outer perimeter.

A minimum required separation distance of 3 mm from all EC structure resulted in the need for two different structure forms. The tall and thin central assemblies were raised approximately 1 cm above the mounting plate by integrated stand-offs, in order to avoid interferences with other structures. The shorter and wider exterior canisters rested directly on the plate and were limited in size by the spring on the VBB sensor elements. Both getter package types consisted of six components: a canister base, a main structure body, a canister lid, a porous membrane filter, and two filter support screens. The 1 µm unsupported porous polytetrafluoroethylene (PTFE) membrane filters acquired from Sterlitech Corp. functioned over the $-120\,^{\circ}C$ to $+260\,^{\circ}C$ thermal range and provided adequate laminar and molecular gas flow. All other structural components were manufactured from titanium alloy Ti-6Al-4V. Figure 2 provides an isometric, sectioned, and exploded CAD views of the central getter packages (a through c), and an image of the development central container next to a ZLA core removed from it (d).

Table 2 summarizes the mass and volume properties of each assembly. The occupied by the ZLA composite volume and the average mass of the complete canister with the getters are given in parentheses.
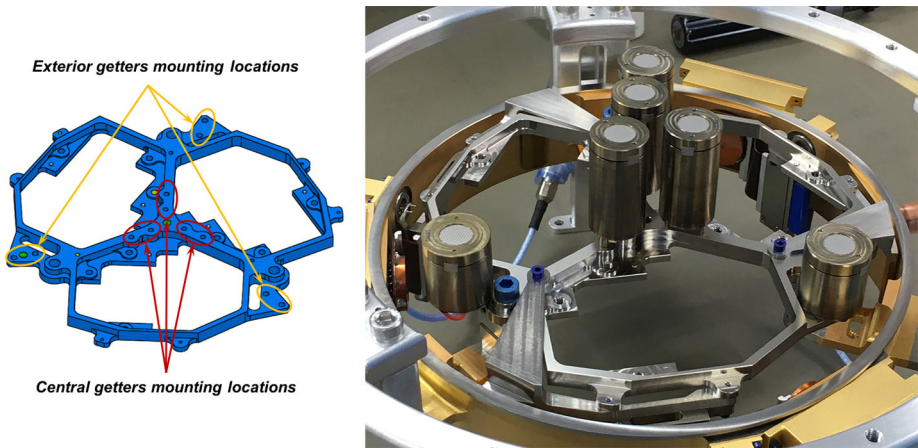
Fig. 1 EC mounting plate with exterior and central getter mounting locations (left) and flight instrument plate with assembled getters (right)
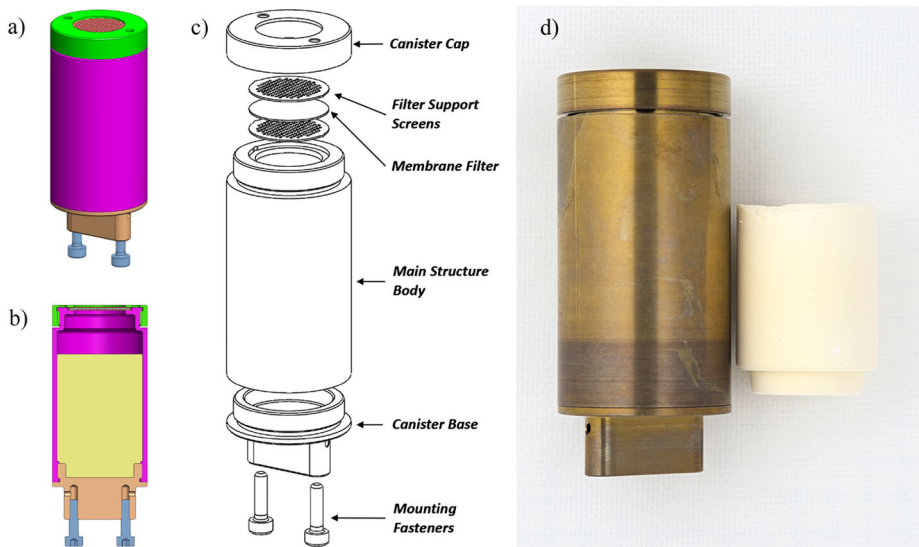

Fig. 2 Isometric (**a**), sectioned (**b**), and exploded CAD views (**c**) of the central getter assembly, and the development getter (**d**) unit adjacent to a ZLA composite molded in the canister shape

The main structure body components of the getter packaging (shown for the exterior getter in Fig. 3a) had internal and external M-profile extra-fine threads at each end, per ASME B1.13M. The canister base and canister lid threaded onto the main structure body (Fig. 3b) and were torqued to a specified limit with a spanner wrench tool using pin hole features on the component faces. To avoid outgassing adhesives and lubricants, the threads were lubricated with an isopropyl alcohol wash prior to assembly and relied on friction via torqueing for primary locking. Secondary thread locking was achieved by spot welding the canister base to the canister body at two equally spaced locations around the threaded

Table 2 Dimensions, volume and average mass of the central and exterior getter assemblies without and with the ZLA composite (in parentheses)

Getter assembly	Outer diameter (mm)	Height (mm)	Internal volume (cm^3)	Average mass (g)
Central	45.9	20.2	7.87	17.9 [18.5]
Exterior	25.25	22.8	5.53	16.1 [16.5]
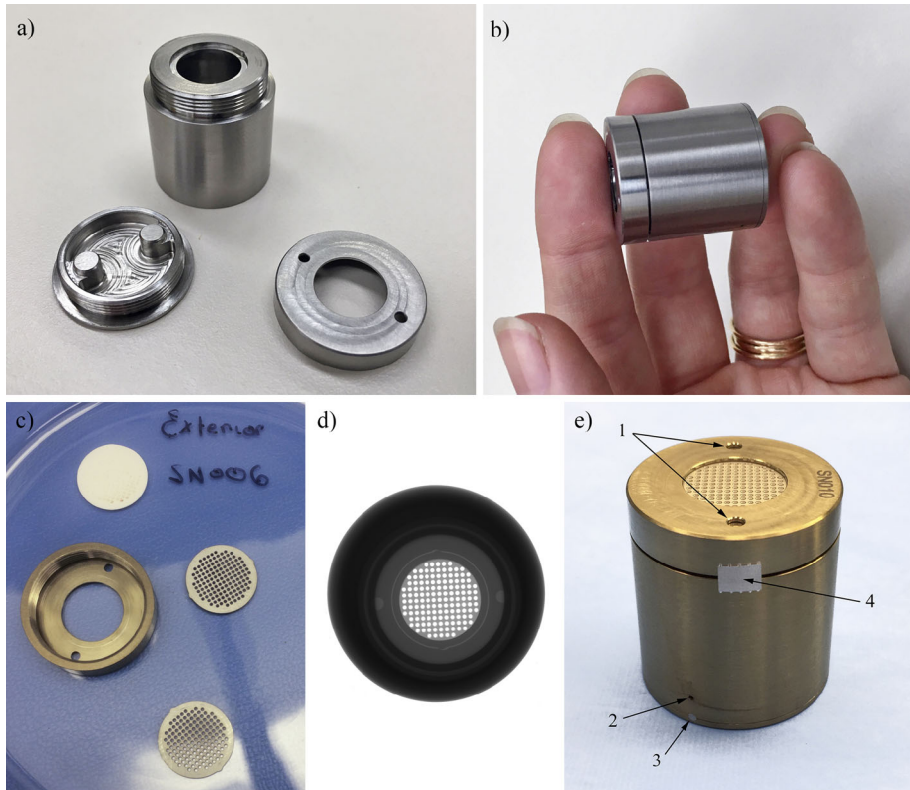
Fig. 3 Exterior getter package images: (**a**) as-built canister body components, shown assembled (**b**) in a relative size comparison; (**c**) 1 µm pore size membrane filter and the two support screens of a development getter after vibration testing; (**d**) the alignment of the holes of the two support screens seen in an X-ray image, and (**e**) fully assembled flight-like getter. The latter shows (1) design features for torqueing, (2) thread venting and (3, 4) secondary thread locking

base joint, and by securing the canister cap to the canister body with two weld straps that span the gap found at the upper threaded joint. Both the interior and exterior assemblies included a 0.5 mm vent hole through the structures' blind threaded interfaces, eliminating the potential for trapped air in the mounting holes. Two titanium support screens (Fig. 3c) with aligned hole patterns clamped and secured the particle filter between the canister lid and main structure body. Protruding features on the screens paired with cut-outs in the canister body acted as hard-stops that prevented the screens from rotating and tearing the filter during the assembly process. The alignment is seen in the X-ray image (Fig. 3d). Figure 3e shows the flight-like assembly and identifies the design features discussed above.

4.2 Filter Conductance Considerations

The getter adsorption rate depends on the filter conductance, molecular transport through the ZLA mesoporous network and adsorption rate on zeolite particles. Evaluation of the filter conductance in the laminar flow regime, which is prevalent during the initial evacuation of the instrument, was done by a differential pressure measurement of air pumped through a filter-covered aperture. The result, scaled to the open filter area of one canister, was 1 L/s, which is half of the conductance of the queusot. This avoids conditions for significant positive differential pressure buildup inside the canisters, which can cause filter damage. One canister was pumped down more than 10 times without noticeable changes to the filter appearance.

General conductance considerations imply that molecular transport through the ~ 1 μm filter holes is significantly faster than that through the 10–100 nm aerogel mesopores of the ZLA bulk. While the knowledge of the actual conductance value is not essential, it was important to demonstrate that the effective filter/ZLA series conductance was adequate to cope with the SEIS outgassing load. This was assessed using the getter adsorption characterization system by introducing high gas load for a period of time and monitoring the subsequent pressure recovery rate due to getter adsorption in the closed vacuum system (Petkov and Soules 2018a). The estimated ~ 15 mL/s conductance at 10^{-3} mbar yielded 1.5×10^{-5} mbar L/s gas throughput capacity for one getter, or just under 1×10^{-4} mbar L/s for the set of six SEIS getters. This exceeds the SEIS outgassing rate by nearly three orders of magnitude, hence proving the adequate filter conductance even for accelerated adsorption tests.

4.3 Compliance with Particle Contamination Requirements

The function of the SEIS getter packages was to ensure the getters compliance with the particle cleanliness level (PCL) instrument requirement of PCL 100 (per IEST-STD-CC1246E), defined as a particle size distribution with a maximum of one 100 μm particle per 0.1 m^2. Thus, the survivability of the ZLA composite under relevant environments was decoupled from its adsorption characteristics, which are unaffected by the material integrity. The stringent PCL 100 requirement was applied to all components inside the EC. It was imposed to minimize the low-probability but potentially high mission risk of a 20 μm-sized particle falling into a critical location that could render a VBB sensor inoperable. In turn, that would severely impact the SEIS quake signal detection capabilities.

Throughout the development process, packaged ZLA getters were subjected to extreme thermal cycling and relevant random vibration environments, and the ZLA cast was subsequently inspected. Unsurprisingly, thermal cycling showed no effects, as the material is capable of withstanding thermal shock in the extreme Mars-applicable range. The more matured product showed good material integrity and adhesion to the canister walls after vibration tests, but particle generation was noticed around the original precursor meniscus area. While the good overall ZLA composite survivability in relevant environments may be acceptable in most cases, the 1 μm pore size membrane filters of the getter canisters were crucial for ensuring the PCL 100 compliance for SEIS. As an example of that, a packaged getter was exposed to a severe shock with a peak response as high as 2000 gpk in the shock response spectrum (SRS) method at 2800 Hz. Not a single zeolite or silica particle was found in a scanning electron microscopy (SEM) examination of the entire getter filter, screen or canister lid surfaces.

All packaged getters were qualified in relevant thermal, vibration and shock environments. The selected levels for component testing included a conservative margin with respect to the instrument-level conditions. Three-axes random vibration testing was done with the InSight frequency profile to and overall response > 10.3 grms, and the three-axes shock testing exceeded peak response of 705 gpk SRS at frequencies greater than 1500 Hz. Thermal qualification testing was done in the -120 °C to $+140$ °C range. A pair of one central and one exterior getters was subjected to additional 30 slightly less severe thermal cycles under a suitably constructed packaging qualification and verification (PQV) test.

Particle count assessment was done at the beginning and after each step of the qualification and PQV programs. Extractive particle sampling was performed on getter surfaces using PTFE type tape-lifts, since the use of adhesive tapes on intrinsic to the EC surfaces was prohibited and rinsing in a liquid could compromise the ZLA composite integrity. This sampling method has limitations due to the lack of adhesive, manifested in less particles removed from a surface in comparison with adhesive tape-lifts or rinse methods. Although not as effective, PTFE tape-lifts delivered sufficient particle count and the method was developed to provide adequate information. All samples taken throughout the qualification and PQV programs complied with the PCL 100 requirement.

5 ZLA Development and Testing

5.1 Composite Development

A comprehensive report on the development of the ZLA composite (Petkov et al. 2018b) elaborates in detail on the results given in this section. The process began with the incorporation of zeolite powders into a two-step sol-gel process for producing silica aerogel developed by Tillotson and Hrubesh (1992). For hydrophilic silica aerogels, a tetraethyl orthosilicate based sol was first prepared using acetonitrile as a solvent. A liquid aerogel precursor was then made by mixing the sol with acetonitrile, water and ammonium hydroxide. The solvent-to-sol proportion determined the final aerogel density. The amount of ammonium hydroxide added determined the gelation time. ZLA composites were made by mixing zeolite particles and fumed silica in the liquid precursor. The microstructure of fumed silica is nearly identical to that of the dried aerogel and served to increase the viscosity in the fluid, which prevented the settling of the zeolite particles prior to gelation. The micron-sized zeolite particles tended to adhere to the large fumed silica particles, which aided in their homogeneous dispersion. The optimization of the zeolite dispersion in the liquid precursor and the manipulation of the gelation speed were key factors in the ZLA composite fabrication.

Throughout the development phase, the liquid zeolite-loaded precursor was cast in a pair of development containers, one central and one external, and the amount of zeolite loading and fill amount for each container were varied. Witness samples were made with each production run for material characterization. Gelation typically occurred within 1–2 hours, but the wet gels were allowed a day to react thoroughly. At this stage, the material consisted of sparsely scattered zeolite particles locked in solid mesoporous silica network, whose pores were filled with acetonitrile solvent. The liquid gel was then dried at temperatures and pressures (295 °C/5.5 MPa) well above the supercritical solvent conditions for acetonitrile (272 °C/4.87 MPa) to avoid vapor-liquid phase drying, which would cause pore collapse. Supercritical drying preserved the original solid network microstructure set in the wet gel.

The material was then heated post-production to 350 °C in dry N_2 atmosphere for a minimum of 72 hours to remove the acetonitrile residue trapped by the zeolites. Subsequently, no acetonitrile fragments or any outgassing products other than water were detected by RGA upon heating the samples to 160 °C in $< 10^{-9}$ mbar vacuum.

The aggressive project schedule put severe restrictions on the scope of the research, which was limited to one of each HY, NaY and CaX commercially available synthetic faujasite materials at the time. No efforts were made to investigate the adsorption as a function of the exchanged cation amount, SiO_2:Al_2O_3 mole ratio, or the microstructure of other zeolites. The raw HY, NaY and CaX powders exhibited moisture adsorption capacity of 25.5 wt.%, 29.0 wt.%, and 27.9 wt.%, respectively. Since the specific capacities were similar, the HY emerged as most suitable to our application due to its lowest water desorption temperature. The integration of the HY zeolite in the aerogel, however, resulted in suppressed capacity, attributed to acetonitrile loading of its more abundant micropores. Henceforth, the primary investigation and development efforts were focused on NaY ZLA composites. CaX, which has a very similar specific adsorption capacity, was included at the end for enhanced CO and CO_2 adsorption.

Isopropyl alcohol and acetone were assessed as alternative solvents in the sol-gel process. This was easily done since they are also in a supercritical state at 295 °C and 5.5 MPa. Samples with identical zeolite loads were produced with the three solvents and were dried at the same time. In addition, a sample made with acetone was dried in a small CO_2 autoclave for comparison. None of these approaches yielded significant benefits with respect to the standard acetonitrile process. The CO_2-dried sample at ~ 40 °C exhibited potential advantages as the dry composite gel material did not contain acetonitrile residue, which likely reacts with zeolites at high temperatures. This warrants further investigation for future applications; however, the small experimental apparatus used at the time could not sustain the large volume production needed for InSight. Since the dry N_2 post-production cleaning step removed the residual acetonitrile and produced similar specific getter capacity, we selected the standard acetonitrile sol-gel process for the production of the flight getters.

The investigation of the getter capacity as a function of the zeolite load was done with NaY ZLA and assessed by thermo-gravimetric analysis (TGA). Note that TGA measurements cannot distinguish between ambient moisture adsorption on the aerogel matrix or the zeolite particles. Hydrophobic aerogel composites were also produced and tested, but material development was not pursued due to the unknown effects of the prevalent organic (CH_3) fragments, which may consume zeolite capacity. A composite plot of multiple different production runs showed an excellent linearity above 30 g/L zeolite load in the liquid precursor (Fig. 4). Below that value, the results were probably affected by aerogel/silica drying under flowing N_2 in the TGA chamber. Due to the additive nature of the zeolites in the composite, it is reasonable to expect that the linear dependence extends to zero zeolite loads, and the offset accounts for adsorption on the aerogel and fumed silica surfaces. The TGA results were used only to guide the material development in parallel with vacuum testing. The quantitative evaluation of the ZLA adsorption capacity was carried out in vacuum since aerogel does not retain moisture below 100 mbar (Richter and Lipka 2003).

The goal of the ZLA development for InSight was to produce a material with the minimum amount of zeolite load that complies with the allocated pressure budget. Lower zeolite loading relaxed the bakeout duration constraints, while attaining < 0.01 mbar PAL ensured excellent vacuum in the EC throughout the mission, including any conceivable mission extension.

Fig. 4 Adsorption capacity of NaY ZLA composites, measured by TGA, as a function of the zeolite loading in the liquid precursor. Each production run is denoted by a different symbol
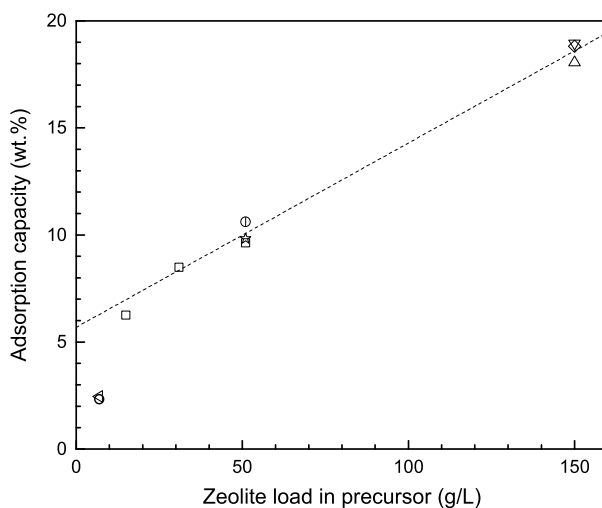
5.2 Adsorption Testing Setup and Method

Vacuum testing of the ZLA composited was evaluated in a custom-designed UHV system described elsewhere (Petkov and Soules 2018). The reference gives details of the measurement methodology and important systematic effects. The test system had a volume of 10.4 L, base pressure of $\sim 2 \times 10^{-10}$ mbar, and an outgassing rate of non-adsorbable gases (H_2) below 1×10^{-9} mbar L/s. The system was comprised of two sections, which can be isolated by gate valves. One of the chambers contained the ZLA getter under test packaged in its SEIS container. Gas transport to the getter occurred through the 1 µm pore size filter (see Sect. 4). The getter was placed on a heater stage facilitating localized bakeout. The second chamber section was used for setting the gas load. Vapors of Nanopure deionized (18 MΩ cm ionic purity) and outgassed-in-vacuum water, introduced through a variable leak valve, were used as a proxy for simulating outgassing from relevant materials. For each setting, the water gas load was determined by the pressure-rise method using micro-Pirani pressure sensor in the sealed section separated from the getter chamber. The micro-Pirani vacuum gauge was the only commercially available option providing good sensitivity, stability, and high reproducibility in the 10^{-5}–1 mbar range and, most importantly, does not affect the measurement (in contrast to ionization gauges). Once the gas load was satisfactorily established after properly accounting for systematic effects due to water adsorption on the system walls, the gate valve between the gas injection chamber and the getter chamber was opened. The ZLA getter provided the only pumping mechanism in the system, disregarding initial adsorption on intrinsic system surfaces for which the results were corrected.

Prior to each test, the UHV system and getter under test were vacuum baked to remove the resident moisture. The bakeout temperature was first set at 120 °C but was later reduced to 100 °C to replicate the constrained SEIS bakeout conditions imposed to minimize the Albefilm 550 outgassing. Typically, a 24 hour-long bakeout sufficed to ensure mid-10^{-10} mbar pressure at RT at the start of each adsorption test. Since water vapor was injected during the experiments, the moisture removal from the intrinsic system surfaces was of secondary importance. The post-bakeout pressure, however, was indicative of the dehydration state of the zeolites in the getter. Most of the moisture was removed within the 24-hour bakeout period, but complete dehydration of the ZLA composites, which generated the maximum

adsorption capacity for a given zeolite loading, required a week-long bakeout. In the interest of faster experimental turnaround times, all getters under test were baked out for 24 hours, and the remaining unliberated adsorption capacity was treated as margin.

The vacuum experiments represented an accelerated adsorption test. The pressure evolution in the system as a function of time was used to derive the performance of the six-getter set in the SEIS instrument using two acceleration factors, accounting for the differences in getter volumes and gas loads in SEIS and in the test setup. The use of the same exterior getter container and cast ZLA amount (with different zeolite loading) in all adsorption tests resulted in a constant getter volume factor of 6.9, calculated as the ratio of flight-to-test ZLA composite volume (26.7 cm^3 and 3.87 cm^3, respectively). The gas load acceleration factor, which varied significantly, was the ratio of the water vapor leak rate in a given test and the SEIS outgassing rate, accepted as 1×10^{-7} mbar L/s for the purpose of the ZLA composite development.

Although very large gas load acceleration factors were conducive to faster experimentation, water vapor injection rates significantly exceeding the getter adsorption rate caused severe deviation from equilibrium conditions. This resulted in excessive pressure buildup in the system, which could lead to gross underestimation of the getter adsorption capacity. Quantification of the getter capacity under non-equilibrium conditions invoked more complex considerations due to the difference of the SEIS and test system volumes and required knowledge of the zeolite adsorption rate at ambient temperatures, which was lacking. A feasibility test with injection rate exceeding equilibrium conditions by two orders of magnitude was demonstrated with 150 g/L NaY ZLA (Petkov and Soules 2018a). The getter continued the adsorb long after the water injection was terminated. Although crude estimates validated excessive adsorption capacity, accurate assessment was hindered by the inherent deficiencies of the non-equilibrium test conditions.

Subsequent testing continued with 51 g/L NaY ZLA composites in quasi-equilibrium conditions. These were determined by lowering the water vapor injection rate until no significant pressure drop was detectable after terminating the water flow. Conservation laws under such circumstances rule that gas flow through the getter filter was greater or equal to the water injection rate. Quasi-equilibrium conditions were attained for injection rates below 10^{-5} mbar L/s.

Multiple adsorption tests with 51 g/L NaY ZLA composites exhibited capacity ensuring compliance with the PAL budget allocation for many years, well in excess of the required 14 months for SEIS. To further relax the bakeout constraints, the zeolite load was gradually reduced to $\sim$ 7.2 g/L. After verification of adequate performance of that ZLA material in multiple adsorption experiments, the zeolite load was split equally between NaY and CaX zeolite powders in order to enhance the CO/CO_2 adsorption without noticeably sacrificing water capacity. The final adsorption tests were conducted with that InSight ZLA composition.

5.3 InSight ZLA Composition and Testing

The InSight ZLA composite was based on 7.2 g/L of 1:1 NaY:CaX mixture zeolite loading in the precursor. The Na-exchanged 13X zeolite (NaY), acquired from Alfa Aesar, had a 5.1:1 SiO_2:Al_2O_3 mole ratio and 900 m^2/g BET surface area. The Ca-exchanged zeolite (CaX) was Grace Sylobead MS544 13X zeolite-X molecular sieve beads (unspecified SiO_2:Al_2O_3 mole ratio or specific surface area), which were crushed to micron-sized powder with mortar and pestle. The anhydrous density of this ZLA composite, measured by the volumetric method (Petkov and Jones 2016), was 113 ± 2 mg/cm^3. The dehydrated zeolite

load, calculated using the precursor composition and respective zeolite powder adsorption capacities accounted for 5.6 g/cm^3, equivalent to 5.0 wt.% zeolite in the ZLA composite. This was corroborated by energy dispersive X-ray (EDX) analysis and X-ray fluorescence (XRF) analysis (Petkov et al. 2018b).

The net weights of the ZLA composite in each of the external and central containers was measured on a microbalance and recorded in the JPL getter flight-built documentation. Using the ambient material density (accounting for 4.5 wt.% H_2O), these values yielded 5.03 cm^3 and 3.87 cm^3 average ZLA composite volume in the central and exterior containers, respectively. Note that both type canisters were underfilled (compare to available canister volumes in Table 2) to achieve better material integrity during mechanical vibration and shock testing. The total ZLA composite volume within SEIS was thus 26.7 cm^3. This corresponds to 3.0 g anhydrous composite weight, which contains only 150 mg zeolite material.

5.3.1 Water Vapor Adsorption

The adsorption of water vapors in vacuum by the InSight ZLA getter composite was tested in quasi-equilibrium conditions using a range of low-rate water injection rates (Petkov et al. 2018b). The adsorption capacity was reported there as adsorbate mass versus zeolite 13X mass in the composite for direct comparison to other zeolite materials, such as zeolite 4A (Gorbach et al. 2004). Here we show the pressure profile evolution over time with a system containing a getter exposed to constant gas load (Fig. 5, solid line). The water vapor injection rate was set and measured by the pressure-rise method at the beginning of the experiment and was remeasured at the end (feature at $\sim$ 87 h) to verify that the gas flow was reasonably constant. Higher injection rates facilitated more constant flow, whereas lower rates exhibited significantly larger variability attributable to known deficiencies in the variable leak valve design. Results with $> 10\%$ difference in the measured rates throughout the experiment were not taken into account in the capacity calculations. For the data shown in Fig. 5, the leak rate values at the start and the end of the experiment were 3.65×10^{-6} mbar L/s and 3.90×10^{-6} mbar L/s, respectively, yielding an acceptable change of 7%. A linear pressure increase in a system without getter (no getter acceleration factor) is shown with a dashed line. The ratio of system (10.4 L) to SEIS volumes (3.3 L) was used to plot that dependence on the same time scale.

The shaded area represents the 14-month SEIS equivalent time, scaled to the experimental clock by the acceleration factor of 257 calculated from the test parameters. From Fig. 5, the predicted pressure value at the time of launch (pressure at the end of the shaded area) was < 0.002 mbar for the assumed 1×10^{-7} mbar L/s SEIS outgassing rate. The pressure-time dependence in the forecast is non-linear. To accommodate the factor of two uncertainty in the outgassing rate determination in a conservative approach, all adsorption experiments continued for at least twice the SEIS equivalent time. The pressure after twice the SEIS equivalent time was $\sim$ 0.004 mbar, still remaining compliant with the budget allocation requirement. This extended time under test method was used to build adsorption capacity margin in the InSight ZLA getters.

A pressure forecast (Fig. 6) based on the above experiment is a relevant representation of getter performance from the mission assurance and project perspective. The data from Fig. 5 were scaled to 2×10^{-7} mbar L/s (grey line) water vapor injection rate, fitted (red line), and the fit was scaled to 1×10^{-7} mbar L/s (black line), and 5×10^{-8} mbar L/s (blue line) outgassing rates, respectively. The two higher and lower rate values represent the bounds of the SEIS outgassing rate, encompassing all measurements. The pressure forecast starts from

Fig. 5 Pressure profile (solid
line) during an adsorption
capacity test of one exterior SEIS
getter under a constant water
vapor flow at RT. The injection
rate was set and measured at
$t = 0$ and remeasured at the end
of the test ($t \sim 87$ h). The dashed
line shows the pressure in the
system for the same water
injection rate in the absence of a
getter on the same time scale.
The hatched area indicates the
14-month SEIS-equivalent time,
scaled with the test acceleration
factor, and the dotted line at
10^{-2} mbar denotes the pressure
budget allocation
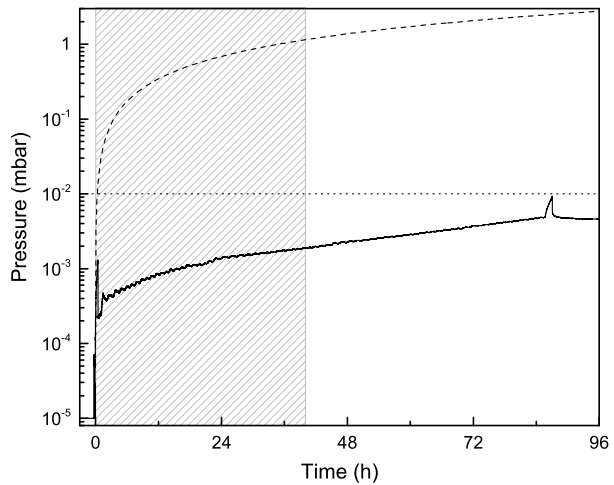
Fig. 6 SEIS pressure forecast at
RT created using the data from
Fig. 5 (grey), scaled to
2×10^{-7} mbar L/s (red),
1×10^{-7} mbar L/s (black), and
5×10^{-8} mbar L/s (blue)
outgassing rates. The ordinate
extends to the PAL allocation
budget. The lower and higher
rates give the bounds of the
measured SEIS outgassing rate.
In situ measurements by the
CNES method are shown with
circles. The method's reliable
sensitivity threshold of
$> 2 \times 10^{-3}$ mbar (dashed line)
was not reached, but the data are
consistent with the forecast based
on adsorption experiments
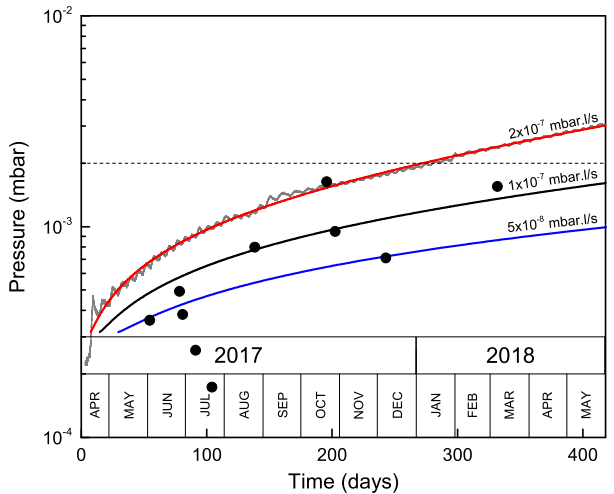
the date of SEIS pinchoff, April 8, 2017, and extends to the end of the launch window. The
InSight mission was launched on May 5, 2018. Recall that the worst pressure in the instru-
ment is built up at the time of launch, and subsequent temperature decrease reduces both,
material outgassing and pressure. With the lack of a direct pressure measurement, the only
in situ pressure verification was done with a Pirani-type gas heat transfer method, developed
by CNES. The method utilized Joule heating of activated VBB motors and monitoring the
time-dependent heat propagation to different locations within SEIS, which resulted in re-
producible sensitivity at $> 2 \times 10^{-3}$ mbar in calibration tests. This technique was used to
measure the intrinsic instrument pressure immediately after pinchoff and at multiple other
instants throughout the instrument integration process (Fig. 6, circles). The last measurement
occurred on March 6, 2018. Although the method's validity range was never conclusively
reached, the noticeable pressure trend in the data was consistent with the pressure forecast.
This puts the pressure estimate in the instrument at launch at around 0.002 mbar, well within
the 0.01 mbar allocated budget.

Fig. 7 Pressure profile (circles) in the UHV test system under constant CO_2 flow rate. The dashed line is the expected pressure without getter, and difference (solid line) represents the adsorbed CO_2 amount on the getter
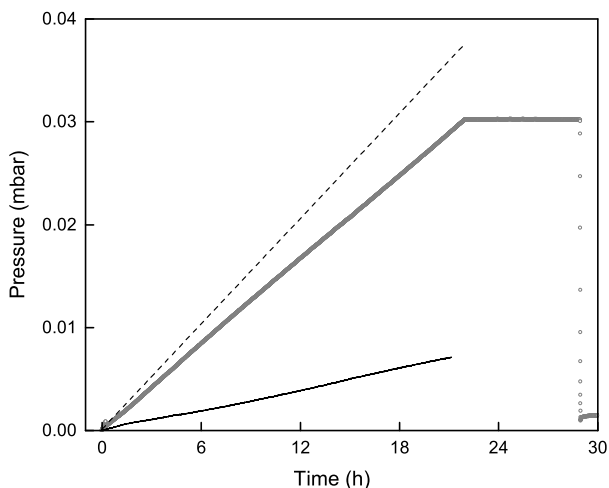
5.4 CO_2 Adsorption

From mission assurance perspective, CO_2 adsorption capability was not an obligatory attribute for the InSight ZLA getters to guarantee the compliance with PAL and EOL requirements. Nevertheless, such a capability was built in for risk mitigation against a physical leak on Mars, without noticeably compromising the moisture adsorption functionality. In general, Ca-exchanged zeolites of a given type (e.g., CaX zeolite 13X) have a significantly higher affinity for CO_2 adsorption with respect to that of Na-exchanged ones (NaY zeolite 13X). The H_2O capacity of the NaY and CaX powders used in this work differed by merely ~ 1 wt.%, which was insignificant considering the large adsorption capacity margin in the NaY ZLA getter tests. Although the 1:1 NaY:CaX zeolite mixture was chosen in this proportion somewhat arbitrarily, the half-load NaY capacity alone (3.6 g/L) was sufficient to guarantee the PAL requirements. Time constraints prohibited month-long CO_2 adsorption testing of NaY ZLA composites for a direct comparison to the InSight NaY:CaX ZLA material, but the CO_2 adsorption capability of the latter was characterized (Petkov et al. 2018b).

Test results from the CO_2 adsorption capacity experiment with the InSight ZLA getter are shown in Fig. 7. Prior to this test the system was subjected to a four-week-long bakeout to remove any residual moisture in the getter and in the system. The role of the moisture was deemed critical since it is readily adsorbed by the getters, and any competition with the CO_2 for common adsorption sites would skew the results. After the bakeout, the system pressure was largely dominated by hydrogen, and the upper limit of the gas load from the non-adsorbable gases was bounded to $< 1 \times 10^{-9}$ mbar L/s. The data in Fig. 7 were obtained with 5×10^{-5} mbar L/s CO_2 injection rate.

In contrast to any moisture adsorption test (e.g., Fig. 5), the CO_2 experiments showed strong pressure-rise linearity. This was due to the non-interacting nature of the CO_2 with intrinsic system surfaces. Quasi-equilibrium conditions were also attained at orders of magnitude higher gas injection rates. Another important difference is that in water adsorption tests, the pressure in the system accounted for a negligible amount of water in comparison with that adsorbed on the getters, whereas the InSight ZLA getters adsorbed only a fraction of the available gas in the system. We infer from the lack of pressure change after termina-

tion of the gas flow (Fig. 7) that the adsorption of CO_2 is proportional to the CO_2 pressure and was not caused by non-equilibrium conditions while the gas was flowing.

The adsorbed amount of CO_2 on the getter (Fig. 7, solid line) was used to estimate the extent of the getters leak mitigation capability under Mars surface conditions. The ZLA composite getters could overcome atmospheric gas influx approaching that of a gross leak which, converted to He equivalent rate as it would show in a conventional test, was $\sim 1.5 \times 10^{-5}$ mbar L/s atm.-He. As a reference, this corresponds to a leak through an aperture with a diameter of ~ 0.3 μm. The CO_2 adsorption rate would be moderately higher on Mars at the instrument operation temperatures.

6 Summary

This article describes the development and implementation of a primary sorption pump to maintain high-vacuum conditions in the SEIS seismometer on the NASA InSight mission to Mars. Within five months, the ZLA composite getter idea was developed from a Technology Readiness Level (TRL) 1, to a TRL 6 sorption pump through validation and verification (V&V) ground testing. Having complied with the PAL allocation requirement, which is the worst-case vacuum condition in the instrument, the technology has achieved TRL 8 at the time of InSight launch. Barring unforeseen anomalies, since compliance with the PAL budget guarantees high vacuum condition in SEIS for many decades on Mars, an argument can be constructed that the ZLA getter technology is mission-proven (TRL 9).

The principal element of the InSight sorption pump was zeolite-loaded aerogel composite material, comprised of micron-sized zeolite particles sparsely and homogeneously distributed throughout a mesoporous aerogel matrix. The ZLA composites are strong lightweight (~ 0.1 g/cm^3) materials with tunable adsorption characteristics to the specific outgassing needs through the choice of embedded zeolite constituents. The porous bulk provides fast molecular diffusion for adsorbate to reach the zeolite adsorbent, whose specific capacity is maximized by avoiding the use of a microporous binder.

The InSight ZLA composite getter pumps were designed to maintain high-vacuum conditions in SEIS for a mission of any duration. Their adsorption properties were optimized primarily for H_2O adsorption, but also have strong affinity for CO, CO_2, organic volatiles, and other adsorbates. We characterized the H_2O and CO_2 adsorption of flight-like ZLA getters in high-vacuum conditions and provided experimental evidence of their performance. The produced flight getters could sustain < 0.01 mbar pressure for several years at RT. The low operational temperature on Mars would act to reduce the SEIS pressure by several orders of magnitude due to enhanced getter performance ($> 10\times$), reduced outgassing from adhesives (10–$100\times$), adiabatic cooling of the gases in the EC volume ($\sim 200\times$ for H_2O), and adsorption on intrinsic SEIS surfaces. A total amount of 3 g ZLA composite containing 150 mg zeolite material is anticipated to maintain the instrument pressure significantly below 10^{-5} mbar throughout any foreseeable mission duration. This eliminates the VBB noise contribution due to gas heat transfer and Brownian molecular motion. The ZLA getters would also be capable of overcoming a significant leak on Mars should that be precipitated by an unforeseen anomaly.

The successful implementation of the ZLA getters in SEIS was aided by the packaging approach. This separated the compliance with the extraordinarily stringent particulate contamination requirements throughout environmental and life tests, which was linked to the getter container integrity, from the adsorption requirements, which remained with the getters.

Due to their inherent cryogenic properties, the ZLA composite getters are exceptionally well suited for application in instruments operating in cold space environments, such as these on the surface of Mars or the icy worlds. These getters are passive adsorbers with a myriad of inherent benefits, such as tunable adsorption characteristics, low mass, no moving parts, no power consumption, no maintenance requirements, no magnetic, electric or thermal interference, etc. Their simple production method allows the ZLA material to be molded into any shape utilizing effectively available space. Sufficient activation of the adsorbent is achieved under standard bakeout conditions such as these required by Planetary Protection protocols. The InSight getters were developed to maintain high vacuum environment ($< 10^{-5}$ mbar) in a sealed instrument, but further material development for sustaining ultra-high vacuum ($< 10^{-7}$ mbar) conditions appears conceivable.

References

W.B. Banerdt, S. Smrekar, T. Hoffman, S. Spath, P. Lognonné, T. Spohn, H. Stone, J. Willis, J. Feldman, R. De Paula, R. Turner, S. Asmar, D. Banfield, U. Christensen, J. Clinton, V. Dehant, W. Folkner, R. Garcia, D. Giardini, M. Golombek, M. Grott, T. Hudson, C. Johnson, G. Kargl, B. Knapmeyer-Endrun, J. Maki, D. Mimoun, A. Mocquet, P. Morgan, M. Panning, W.T. Pike, C. Russell, N. Teanby, J. Tromp, R. Weber, M. Wieczorek, K. Hurst, E. Barrett (InSight Team), The InSight mission for 2018, in *48th Lunar and Planetary Science Conference* (2017)

S. De Raucourt, T. Gabsi, N. Tanguy, D. Mimoun, P. Lognonné, J. Gagnepain-Beyneix, W. Banerdt, S. Tillier, K. Hurst, The VBB SEIS experiment of InSight, in *39th COSPAR Scientific Assembly* (2012), p. 429

V. Dehant, B. Banerdt, P. Lognonné, M. Grott, S. Asmar, J. Biele, D. Breuer, F. Forget, R. Jaumann, C. Johnson, M. Knapmeyer, B. Langlais, M. LeFeuvre, D. Mimoun, A. Mocquet, P. Read, A. Rivoldini, O. Romberg, G. Schubert, S. Smrekar, T. Spohn, P. Tortora, S. Ulamec, S. Vennerstrøm, Future Mars geophysical observatories for understanding its internal structure, rotation, and evolution. Planet. Space Sci. **68**, 123–145 (2012)

D. Faye, A. Jakob, M. Soulard, P. Berlioz, Zeolite adsorbers for molecular contamination control in spacecraft, in *Optical System Contamination: Effects, Measurements, and Control 2010*. Proc. SPIE, vol. 7794 (2010), p. 77940B

A. Gorbach, M. Stegmaier, G. Eigenberger, Measurement and modeling of water vapor adsorption on zeolite 4A—equilibria and kinetics. Adsorption **10**, 29–46 (2004)

O. Grosjean, M.P. Petkov, M. Gautherin, A. Lecocq, P.-A. Dandonneau, Vacuum solution approach for the SEIS instrument on the InSight mission to Mars, in *42nd COSPAR Scientific Assembly* (2018 in press)

P. Lognonné, C.L. Johnson, Planetary seismology, in *Physics of Terrestrial Planets and Moons*, ed. by G. Schubert. Treatise on Geophysics, vol. 10, 2nd edn. (Elsevier, Oxford, 2015), pp. 65–120

D. Mimoun, P. Lognonné, W. Banerdt, K. Hurst, S. Deraucourt, J. Gagnepain-Beyneix, T. Pike, S. Calcutt, M. Bierwirth, R. Roll et al., The InSight SEIS experiment, in *43rd Lunar and Planetary Science Conference* (2012)

D. Mimoun, N. Murdoch, P. Lognonné, K. Hurst, W.T. Pike, J. Hurley, T. Nébut, W.B. Banerdt (SEIS Team), The noise model of the SEIS Seismometer of the InSight mission to Mars. Space Sci. Rev. **211**, 383–428 (2017)

J.F. O'Hanlon, High vacuum operation, in *A User's Guide to Vacuum Technology* 3rd edn. (Wiley, New York, 2003), pp. 150–153

M.P. Panning, P. Lognonné, W.B. Banerdt, R. Garcia, M. Golombek, S. Kedar, B. Knapmeyer-Endrun, A. Mocquet, N.A. Teanby, J. Tromp, R. Weber, E. Beucler, J.F. Blanchette-Guertin, E. Bozdag, M. Drilleau, T. Gudkova, S. Hempel, A. Khan, V. Leki, N. Murdoch, A.C. Plesa, A. Rivoldini, N. Schmerr, Y. Ruan, O. Verhoeven, C. Gao, U. Christensen, J. Clinton, V. Dehant, D. Giardini, D. Mimoun, W.T. Pike, S. Smrekar, M. Wieczorek, M. Knapmeyer, J. Wookey, Planned products of the Mars structure service for the InSight mission to Mars. Space Sci. Rev. **211**, 611–650 (2016)

M.P. Petkov, S.M. Jones, Accurate bulk density determination of irregularly shaped translucent and opaque aerogels. Appl. Phys. Lett. **108**, 194104 (2016)

M.P. Petkov, D.M. Soules, UHV system for quasistatic characterization of adsorbers for medium vacuum applications. Vacuum **151**, 254–260 (2018a)

M.P. Petkov, S.M. Jones, G.E. Voecks, Zeolite-loaded aerogel as a primary vacuum sorption pump in planetary instruments. Adsorption (2018b submitted)

D. Richter, D. Lipka, Measurement of the refractive index of silica aerogel in vacuum. Nucl. Instrum. Methods Phys. Res., Sect. A, Accel. Spectrom. Detect. Assoc. Equip. **513**, 635–638 (2003)

G. Rioland, T. Jean Daou, D. Faye, J. Patarin, A new generation of MFI-type zeolite pellets with very high mechanical performance for space decontamination. Microporous Mesoporous Mater. **221**, 167–174 (2016)

M. Takeda, H. Kurisu, S. Yamamoto, H. Nakagawa, K. Ishizawa, Hydrogen outgassing mechanism in titanium materials. Appl. Surf. Sci. **258**, 1405–1411 (2011)

T.M. Tillotson, L.W. Hrubesh, Transparent ultralow-density silica aerogels prepared by a two-step sol-gel process. J. Non-Cryst. Solids **145**, 44–50 (1992)